

Long-term monitoring of the internal energy distribution of isolated cluster systems

Christian Breitenfeldt,^{1,2} Klaus Blaum,² Sebastian George,² Jürgen Göck,² Gregorio Guzmán-Ramírez,³ Jonas Karthein,² Thomas Kolling,⁴ Michael Lange,² Sebastian Menk,² Christian Meyer,² Jennifer Mohrbach,⁴ Gereon Niedner-Schatteburg,⁴ Dirk Schwalm,^{2,5,*} Lutz Schweikhard,¹ and Andreas Wolf²

¹*Institut für Physik, Ernst-Moritz-Arndt-Universität, 17487 Greifswald, Germany*

²*Max-Planck-Institut für Kernphysik, 69117 Heidelberg, Germany*

³*Departamento de Ingenierías, Centro Universitario de Tonalá, Universidad de Guadalajara, Jal. 48525, Mexico*

⁴*Fachbereich Chemie und Forschungszentrum OPTIMAS,*

Technische Universität Kaiserslautern, 67663 Kaiserslautern, Germany

⁵*Department of Particle Physics, Weizmann Institute of Science, Rehovot 76100, Israel*

A method is presented to monitor the internal energy distribution of cluster anions via delayed electron detachment by pulsed photoexcitation and demonstrated on Co_4^- in an electrostatic ion beam trap. In cryogenic operation, we calibrate the detachment delay to internal energy. By laser frequency scans, at room temperature, we reconstruct the time-dependent internal energy distribution of the clusters. The mean energies of ensembles from a cold and a hot ion source both approach thermal equilibrium. Our data yield a radiative emission law and the absorptivity of the cluster for thermal radiation.

Understanding of complex molecules and clusters is governed by the interplay of microscopic description and multistate statistics. Statistical methods were successfully applied to unimolecular reactions (such as dissociation or electron emission) [1] and radiative interactions [2]. Near infrared radiation from nanosystems is important for understanding interstellar continuum emission [3] as well as the survival of molecular matter in the interstellar medium, such as carbon bearing anions [4, 5]. Spectral observations in some wavelength regions point to continuum black-body emission even from very small clusters [6]. On the other hand, it is still not well understood how the emission properties are related to the particles' internal energy distributions [7], even at the higher temperatures investigated so far [6, 7].

Recently, ion-trap experiments could access internal energy relaxation through studies of delayed electron emission from molecular and cluster anions. Time-resolved measurements indirectly demonstrated Stefan-Boltzmann-like relaxation [8] and sampled shifts of internal energy distributions for up to ~ 100 ms [9, 10]. Yet, basic uncertainties remain: Without direct scanning of the internal energy distribution (IED) in a cluster ensemble it is unclear how closely the IEDs follow a canonical shape. Moreover, radiative relaxation was studied only for cluster temperatures high above 300 K [11, 12]. Much less is known at longer observation times and for temperatures where far-infrared emission dominates.

In the present work, we succeed in tracking IEDs in small cluster anions stored in vacuum over several seconds, until the distributions from a hot and a cold ion source both approach thermal equilibrium with the environment. This is achieved by a direct bin-wise measurement of the IED using laser excitation. Single-photon excitation of stored anions by a nanosecond laser pulse increases their internal energy E by the photon energy $h\nu$ from far below the electron affinity EA up to a value

$E' = E + h\nu$ above the EA. Internal conversion [13, 14] quenches the electronic excitation and leads to delayed vibrational electron detachment [1] with an excitation-energy sensitive delay of up to ~ 1 ms [8–10]. On Co_4^- clusters in an electrostatic ion beam trap (EIBT) [15–18] we observe electron detachment in a fixed range of delay after the laser pulse. Operation of the trap at cryogenic temperature [17–19] allows us to determine the range of internal cluster energies that causes photodetachment in the observed delay window. Hence, from the photon energy, we know the internal energy before laser excitation and can scan the IED by photon energy variation.

The IED is measured time-resolved (in 50 ms steps) with bin widths < 0.1 eV. We find near-canonical IEDs with significant deviations for the initially hot clusters up to about 1 s of storage at room temperature. The average internal energies as a function of time follow a modified Stefan-Boltzmann law. The equilibrium internal energy and the relaxation time dependence allow conclusions on the thermal properties of the cluster and its absorptivity for thermal radiation.

The experiments are performed with the Cryogenic Trap for Fast ion beams (CTF), an EIBT at the Max-Planck-Institut für Kernphysik in Heidelberg [17, 18]. Co_4^- anions are produced with a metal ion sputter source (MISS) and a laser vaporization source (LVAP). The MISS is a cesium sputter source yielding clusters at high ro-vibrational energies [20, 21]. In the LVAP [22], 10–20 mJ pulses from the second harmonic of a Nd:YAG laser hit a cobalt target. Cooling the ablated plasma by a short helium pulse (14 bar backing pressure) leads to clustering and supersonic expansion of the helium-cluster mixture through a 2-mm nozzle yields clusters of low internal temperatures [23].

The cluster ions are accelerated to 6 keV, mass selected by a dipole magnet and captured in the CTF. As sketched in the inset of Fig. 1(a), the anions oscillate with the ac-

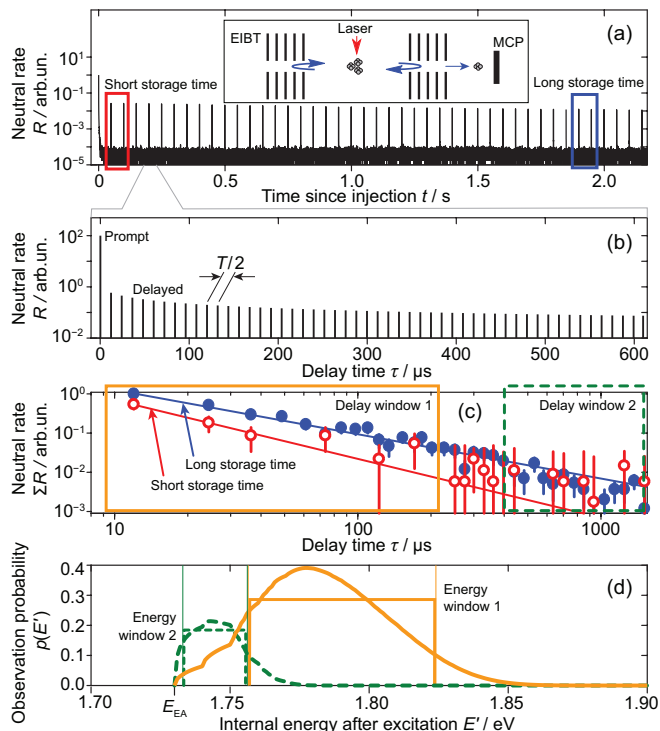


FIG. 1. (a) Co_4^- neutralization rate $R(t)$ (for ions produced by MISS, averaged over $\sim 10^4$ injections) showing hot-ion relaxation after injection ($t = 0$) and peaks induced by laser pulses with $h\nu = 1.55$ eV. Inset: schematic of the EIBT with the mirror electrodes, the crossing laser, and the MCP detector. (b) Schematic laser-probing signal with delayed spikes spaced by half the EIBT oscillation period (T). (c) Summed laser signals ΣR from laser-pulse pairs marked in (a). Solid lines: approximate power-law decays (to guide the eye). (d) Probability functions $p(E')$ for observing neutrals at the MCP (unit detector response assumed) as functions of the internal energy E' after laser excitation [thick solid and dashed curves for the delay time windows marked in (c); thresholds at the detachment energy E_{EA}]. Rectangles: energy windows with the heights marking the averages of $p(E')$ in the E' intervals.

celeration energy over the ~ 30 cm spacing between the electrostatic mirrors. Fast neutrals created by electron emission can leave the trap through the downstream mirror and are monitored by a micro-channel plate (MCP) detector. The count rate R as a function of storage time t [Fig. 1(a)] reflects the internal cluster energies E or E' without or with laser excitation, respectively. The peak at $t \sim 0$, decaying within ~ 10 ms, is due to clusters from the hot source with internal energies E above the EA. Starting 49 ms after each injection and repeated every 50 ms, nanosecond laser pulses from a tunable optical parametric oscillator (OPO) laser are crossed with the stored anions in the trap center. A pulse energy of 1–2 mJ at ~ 1 cm laser beam diameter ensures dominance of single photon absorption.

The clusters, captured as a bunch, disperse over all length and oscillation phases between the EIBT mirrors

within milliseconds. The laser beam overlaps ~ 50 – 1000 , both forward and backward moving anions. Only few of them are excited to $E' = E + h\nu$. For $E' > E_{EA}$, prompt and delayed neutralization occur after a laser pulse. While the average count rates are kept low enough to avoid detector saturation, a signal accumulated over many injections yields the neutralization pulse structure [Fig. 1(a)] on a background from residual-gas induced neutralization.

The fine-structure of these pulses [scheme in Fig. 1(b)] as function of the delay $\tau = t - t_p$ after a laser pulse at probing time t_p reflects the ion oscillations (period $T = 23$ μ s). A prompt spike comprises neutralization within $\sim T/4$ after illumination. Then, similar to earlier experiments [9, 10], spikes delayed by $\tau = nT/2$ (integer n) follow from anions performing n half-roundtrips before electron emission. The spikes of $R(\tau)$ integrate delayed electron emission events that clusters undergo during $\tau \pm T/4$. Spike amplitudes $R(\tau)$ from delayed laser-induced emission are shown in Fig. 1(c). These delayed neutralization rates have the expected [1] approximate power-law time dependence. For the plotted example with $h\nu = 1.55$ eV, they become higher and decrease less rapidly for longer (~ 1.8 s) than for short (~ 0.1 s) probing times. This, at first sight counterintuitive behaviour strongly depends on $h\nu$ as shown below.

In order to have sufficient statistics for efficient monitoring, the event yield is summed over a delay window of $\tau = (12 \dots 200)$ μ s [window 1, Fig. 1(c)]. Importantly, only clusters in a limited range of internal energy E' after laser excitation show electron detachment at such delays. With experimental parameters for delayed electron detachment from Co_4^- described below, we calculate the probability $p(E')$ to observe a neutralization event within the delay window, finding significant likelihood only for anions with E' in an ~ 0.07 eV wide range near ~ 1.8 eV [Fig. 1(d)]. We approximate $p(E')$ by a box whose height gives the average \bar{p} of $p(E')$ between the sharp limits and interpret the delayed yield to follow the number of anions excited to this E' interval by the laser. For longer delays, $p(E')$ is downshifted and lowered. Guided by the variation of $p(E')$ with the delay, we assign the yield in a later window 2 [$\tau = (400 \dots 1500)$ μ s] to an adjacent, more narrow bin of E' [Fig. 1(d)]. Window 2 is included since it improves the energy resolution, but as it has lower statistics, the results are dominated by window 1.

For window 1, Fig. 2 shows the laser-induced yield $Y(h\nu, t)$, i.e., the delayed count rate normalized to the photon number (via the laser intensity), to \bar{p} , and to the stored-ion number [from the background in Fig. 1(a)]. For a set of photon energies $h\nu$ (Fig. 2, legend) and the two ion sources, 10^3 to 8×10^4 injection cycles each were repeated. As the delayed events can be associated with a specific interval of E' , they reflect the IED before laser excitation, denoted by $N(E)$ with $E = E' - h\nu$. As illustrated by Fig. 2(c) the IED, shifted by one-photon

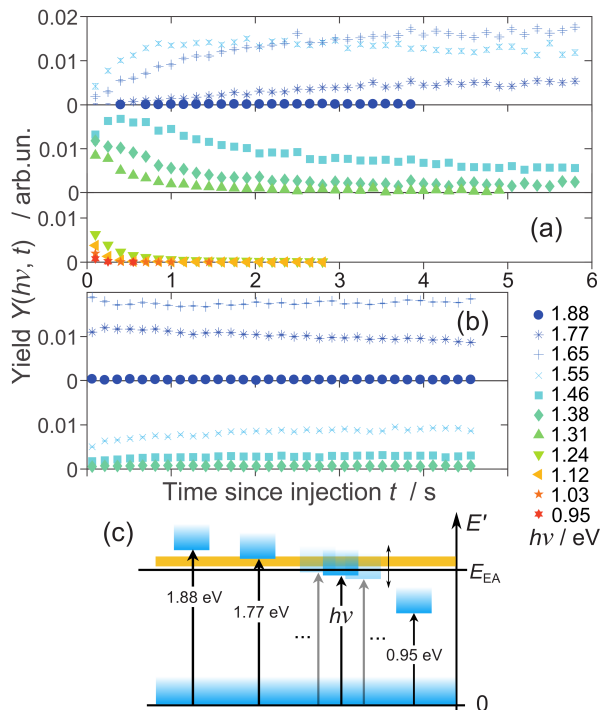


FIG. 2. Normalized yield $Y(h\nu, t)$ in delay window 1 for the listed photon energies $h\nu$ and a scheme of the IED scan. Data for (a) hot (MISS) and (b) cold (LVAP) ion source, averaged over three consecutive probing times. Legend: values of $h\nu$ and their symbols as used in (a) and (b). (c) Scheme of scanning the IED of stored ions (lower shaded band) by laser excitation at varying $h\nu$ (vertical arrows). A bar just above the detachment energy E_{EA} shows the sensitive range of the delayed photodetachment signal.

absorption, is moved over the sensitive E' interval by varying $h\nu$. In fact, $h\nu$ must be low enough for delayed yield to be observed at all: only at $h\nu \leq 1.77$ eV does the low- E range of the shifted $N(E)$ start to overlap with the sensitive E' window. Lower $h\nu$ probe, via the same E' window, higher parts of the IED.

For the hot ion source [MISS, Fig. 2(a)] and low $h\nu$ (< 1.31 eV), yield is found at short t and later disappears as the hot part of the IED relaxes. Signals with 1.46 eV $< h\nu \leq 1.77$ eV grow with t reflecting the increase of the IED at lower energies. In contrast, for the cold ion source [LVAP, Fig. 2(b)] temporal variations are much smaller. Yield at high $h\nu$ (small E) is large already at short t and even slowly decreases, while at lower $h\nu$ (higher E) a slow increase is observed; both indicate how initially colder ions heat up slightly during storage.

The delayed electron emission from a cluster anion with internal energy above E_{EA} is dominated by statistical vibrational autodetachment [1]. To obtain its rate constant $k(E')$, we model this process [1, 24, 25] with vibrational-level densities of Co_4^- and Co_4 from density functional theory. With the level densities and E_{EA} , we derive the $k(E')$ except for a scaling factor k_0 which,

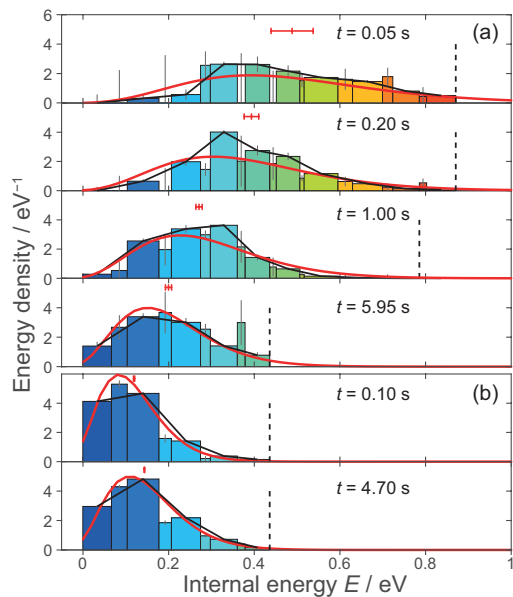


FIG. 3. Normalized histograms $N(E)$ from yields $Y(h\nu, t)$ ($h\nu$ from Fig. 2) for marked probing times, representing IEDs of ions produced with the (a) MISS and (b) LVAP sources. Bin shading encodes $h\nu$. Thin lines: statistical uncertainties of the bin contents. Marks at the top of each panel: histogram averages \bar{E} and their statistical uncertainties. Straight segments connect the data for window 1. Smooth curves: canonical distributions (0.02 eV bins) for harmonic approximation with the respective \bar{E} . Dashed: upper probing energy limit.

together with E_{EA} , is experimentally determined. At $E' \sim E_{EA}$, where $k(E')$ is small, the competition by radiative decay of the excited Co_4^- is accounted for by an energy-independent rate constant k_r . (This radiative decay also influences $N(E)$ with $E \ll E_{EA}$ as probed by the $h\nu$ scan, but at much lower rates.) The model parameters are determined [25] from fits of the calculated neutral-rate time dependence to two subsets of data. The first, studied under cryogenic low-background conditions, is the initial neutral rate of hot (MISS) Co_4^- ions [signal near $t = 0$ in Fig. 1(a)]. The second subset is the average of laser-induced bursts for storage time $t > 3.8$ s. The combined analysis yields $E_{EA} = 1.73(1)$ eV, $k_0 = 240(70)$ s⁻¹, and $k_r = 70(70)$ s⁻¹, from which $k(E')$ and the probability functions $p(E')$ of Fig. 1(d) are derived [25]. The probed internal-energy ranges are $E' = E_{EA} + (0.024 \dots 0.094)$ eV for delay window 1 and $E' = E_{EA} + (0.003 \dots 0.023)$ eV for window 2. For probing times spaced by 50 ms, normalized histograms $N(E)$ of the IEDs are constructed. Here, each $h\nu$ yields a high-statistics bin from window 1 and a narrower, downshifted, but lower-statistics bin from window 2. Small gaps or overlaps between the bins are compensated [25] to uniquely and fully cover the E scale.

Exemplary $N(E)$ are shown in Fig. 3. While $h\nu$ is known to < 0.001 eV, we estimate an uncertainty of

± 0.02 eV in each bin position from the uncertainty of the model for the sensitive E' windows [25]. Smoothed IED curves using canonical level populations within the harmonic model [25], calculated for the same average energies \bar{E} as those of the measured histograms, are superimposed. For the hot ion source [Fig. 3(a)], relaxation of $N(E)$ and improving agreement with the canonical shape are seen, while for the cold ion source [Fig. 3(b)] temporal changes are much smaller with better fit to the canonical shape. Lacking relevant data, we assumed the cross section $\sigma(\nu)$ for single-photon excitation of the Co_4^- anions to be constant over the investigated range of $h\nu$. The absence of sharp resonances appears plausible considering the broadening of electronic transitions by rotational and vibrational excitation and the expected rapid internal conversion. As scanning of $h\nu$ implies scanning of E , unaccounted structures of $\sigma(\nu)$ would cause features in the IEDs repeating for different times at the same E , which is not observed. A steady variation of $\sigma(\nu)$ along ν (and E) cannot be ruled out. With calculated canonical IEDs, we find that a possible factor-of-four [25] variation of $\sigma(\nu)$, assumed to be linear in $h\nu$, causes a further ± 0.02 eV uncertainty in \bar{E} . For the overall uncertainty of \bar{E} we estimate ± 0.03 eV. The experimental binning is estimated (at long t) to upshift \bar{E} by $\lesssim 0.005$ eV.

We derive the mean internal energy \bar{E} from all $N(E)$ histograms [Fig. 4(a)]. They reflect the cooling of the hot ion ensemble and the slow heating up of the cold one. Also, we obtain the squared deviations of the $N(E)$ bin values from the canonical energy density in the same bins. The average of this variance, taken over the primary (high-statistics) bins only, is shown in Fig. 4(b). For the hot (MISS) ensemble, initially large variances shrink and level off during the relaxation, approaching the squared statistical uncertainty of the $N(E)$ bin contents, (0.1...0.2) eV^{-2} . For the LVAP ensemble, the average variance is at the low value of ~ 0.1 eV^{-2} at all times.

The mean energies \bar{E} for the two ion sources [Fig. 4(a)] approach a common equilibrium value. A modified Stefan–Boltzmann law was fitted to the data, assuming the emitted power of an ion ensemble at \bar{E} as proportional to \bar{E}^p ($p = 4$ for the Stefan–Boltzmann case) and, thus, a net power exchange of

$$\frac{d\bar{E}}{dt} = B(\bar{E}_{\text{eq}}^p - \bar{E}^p) \quad (1)$$

with \bar{E}_{eq} the energy at equilibrium with the environment. A combined fit of solutions of Eq. (1) to the MISS and LVAP data yields $\bar{E}_{\text{eq}} = 0.162(2)_{\text{stat}}(30)_{\text{sys}}$ eV, $B = 18(7) \text{eV}^{1-p} \text{s}^{-1}$, and $p = 4.2(3)$, i.e., close to the Stefan–Boltzmann value of $p = 4$.

Observing that the initially hot and cold cluster ensembles both approach the same \bar{E} , we conclude that the internal energy \bar{E}_{eq} is that of a Co_4^- cluster in equilibrium with a thermal bath at the trap temperature

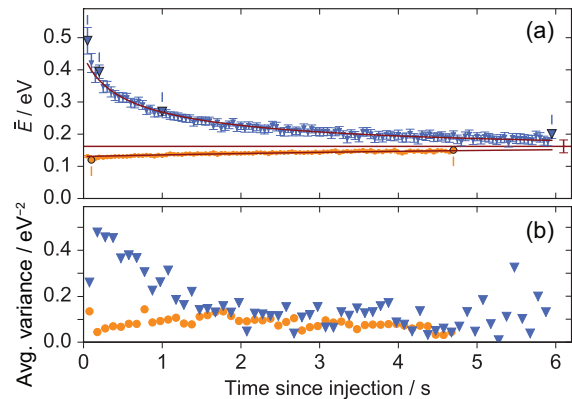


FIG. 4. (a) Average internal energy \bar{E} derived from the measured IEDs for ion sources MISS (triangles) and LVAP (dots) with statistical uncertainties. Full curves: fit using Eq. (1). Horizontal line: \bar{E}_{eq} with the estimated systematic uncertainty. Large symbols and vertical marks: data points for the IEDs of Fig. 3. (b) Average variance between the IED data (bins from window 1) and the canonical energy density averaged over the same bins for ion sources MISS (triangles) and LVAP (dots), averaged over two consecutive probing times.

($T_{\text{eq}} = 295$ K). The vibrational internal energy (caloric curve) of Co_4^- is 0.09(1) eV at this T_{eq} in the harmonic approximation [25] allowing for a $\pm 20\%$ common scaling of all mode frequencies. As the measured \bar{E}_{eq} lies 0.07(3) eV higher, it appears that harmonic vibrations alone do not adequately describe the internal cluster energies under the conditions accessed by the present long-term observations of an isolated cluster. In particular, it neglects isomeric transformations [32, 33], magnetic moments [34], and electronic excitation. The latter, predicted to be > 0.6 eV [33], are likely to be negligible.

From the energy relaxation curves one can infer the absorptivity α of Co_4^- . Equation (1) with $p = 4$ and $\bar{E} \approx CT$, $C = \bar{E}_{\text{eq}}/T_{\text{eq}} = 5.5(1.0) \times 10^{-4} \text{eV/K}$, can be compared to the standard Stefan–Boltzmann law $d\bar{E}/dt = \alpha A \sigma_{\text{SB}}(T_{\text{eq}}^4 - T^4)$ with $\sigma_{\text{SB}} = 3.540 \times 10^{-7} \text{eV s}^{-1} \text{nm}^{-2} \text{K}^{-4}$. Assigning to Co_4^- a surface of $A \approx 0.5 \text{nm}^2$ results in an absorptivity of Co_4^- of $\alpha \approx BC^4/A\sigma_{\text{SB}} \approx (0.25 \dots 2.5) \times 10^{-5}$. Alternatively, α can also be estimated [2] for very small particles to be of the order of their radius ($\sim 0.2 \text{nm}$ for Co_4^- [33]) divided by the wavelength ($\sim 16 \mu\text{m}$ for the peak of 295-K thermal radiation) in agreement with our experimental order of magnitude.

In summary, we demonstrate how single-photon excitation and delay-sensitive electron detachment measurements can be combined for laser-scanning of internal cluster energy distributions with high temporal and energetic resolution. Further studies by this method accessing lower equilibrium temperatures are envisaged at the CTF [35] and the newly developed cryogenic storage rings [36, 37]. With very narrow IEDs realized at these devices,

laser excitation will offer theory-independent calibration of the emission versus internal energy and, thus, application of the method to systems with less knowledge on the relevant level densities.

We acknowledge financial support by the Max-Planck Society and the Max-Planck Förderstiftung. This work was supported by the German research foundation DFG within the Transregional Collaborative Research Center SFB/TRR 88 “Cooperative effects in homo and heterometallic complexes” (3MET.de).

* deceased 14 July 2016

- [1] J. U. Andersen, E. Bonderup, and K. Hansen, *J. Phys. B: At. Mol. Opt. Phys.* **35**, R1 (2002).
- [2] K. Hansen and E. E. B. Campbell, *Phys. Rev. E* **58**, 5477 (1998).
- [3] W. W. Duley, *Astrophys. J.* **705**, 446 (2009).
- [4] E. Herbst and Y. Osamura, *Astrophys. J.* **679**, 1670 (2008).
- [5] C. Joblin, P. Boissel, and P. de Parseval, *Planet. Space Sci.* **45**, 1539 (1997).
- [6] R. Mitzner and E. Campbell, *J. Chem. Phys.* **103**, 2445 (1995).
- [7] Y. Fan, S. B. Singer, R. Bergstrom, and B. C. Regan, *Phys. Rev. Lett.* **102**, 187402 (2009).
- [8] Y. Toker, O. Aviv, M. Eritt, M. L. Rappaport, O. Heber, D. Schwalm, and D. Zajfman, *Phys. Rev. A* **76**, 053201 (2007).
- [9] M. Goto, A. E. K. Sundén, H. Shiromaru, J. Matsumoto, H. Tanuma, T. Azuma, and K. Hansen, *J. Chem. Phys.* **139**, 054306 (2013).
- [10] K. Najafian, M. S. Pettersson, B. Dynefors, H. Shiromaru, J. Matsumoto, H. Tanuma, T. Furukawa, T. Azuma, and K. Hansen, *J. Chem. Phys.* **140**, 104311 (2014).
- [11] C. Walther, G. Dietrich, W. Dostal, K. Hansen, S. Krückeberg, K. Lützenkirchen, and L. Schweikhard, *Phys. Rev. Lett.* **83**, 3816 (1999).
- [12] K. Hansen, Y. Li, V. Kaydashev, and E. Janssens, *J. Chem. Phys.* **141**, 024302 (2014).
- [13] M. Bixon and J. Jortner, *J. Chem. Phys.* **48**, 715 (1968).
- [14] A. Leger, L. D’Hendecourt, P. Boissel, and F. X. Desert, *Astron. Astrophys.* **213**, 351 (1989).
- [15] D. Zajfman, O. Heber, L. Vejby-Christensen, I. Ben-Itzhak, M. Rappaport, R. Fishman, and M. Dahan, *Phys. Rev. A* **55**, R1577 (1997).
- [16] H. Wollnik and M. Przewloka, *Int. J. Mass Spectrom. Ion Processes* **96**, 267 (1990).
- [17] M. Lange, M. Froese, S. Menk, J. Varju, R. Bastert, K. Blaum, J. R. C. López-Urrutia, F. Fellenberger, M. Grieser, R. von Hahn, O. Heber, K.-U. Kühnel, F. Laux, D. A. Orlov, M. L. Rappaport, R. Repnow, C. D. Schröter, D. Schwalm, A. Shornikov, T. Sieber, Y. Toker, J. Ullrich, A. Wolf, and D. Zajfman, *Rev. Sci. Instrum.* **81**, 055105 (2010).
- [18] C. Breitenfeldt, K. Blaum, M. W. Froese, S. George, G. Guzman-Ramirez, M. Lange, S. Menk, L. Schweikhard, and A. Wolf, *Phys. Rev. A* **94**, 033407 (2016).
- [19] S. Menk, S. Das, K. Blaum, M. W. Froese, M. Lange, M. Mukherjee, R. Repnow, D. Schwalm, R. von Hahn, and A. Wolf, *Phys. Rev. A* **89**, 022502 (2014).
- [20] A. Wucher and B. J. Garrison, *J. Chem. Phys.* **105**, 5999 (1996).
- [21] A. Wucher, A. Bekkerman, N. Dzhemilev, S. Verkhoturovb, and I. Veryovkin, *Nucl. Instrum. Methods Phys. Res. B* **140**, 311 (1998).
- [22] S. Dillinger, J. Mohrbach, J. Hewer, M. Gaffga, and G. Niedner-Schatteburg, *Phys. Chem. Chem. Phys.* **17**, 10358 (2015).
- [23] P. Milani and W. A. de Heer, *Phys. Rev. B* **44**, 8346 (1991).
- [24] K. Hansen, *Statistical Physics of Nanoparticles in the Gas Phase*, Springer Series on Atomic, Optical and Plasma Physics No. 73 (Springer, 2013).
- [25] See Supplementary Material at ... for data analysis details and uncertainty estimates, which includes Refs. [26–31].
- [26] B. Kafle, O. Aviv, V. Chandrasekaran, O. Heber, M. L. Rappaport, H. Rubinstein, D. Schwalm, D. Strasser, and D. Zajfman, *Phys. Rev. A* **92**, 052503 (2015).
- [27] S. Martin, J. Bernard, R. Brédy, B. Concina, C. Joblin, M. Ji, C. Ortega, and L. Chen, *Phys. Rev. Lett.* **110**, 063003 (2013).
- [28] J. Troe, T. M. Miller, and A. A. Viggiano, *J. Chem. Phys.* **127**, 244303 (2007).
- [29] T. Beyer and D. F. Swinehart, *Commun. ACM* **16**, 379 (1973).
- [30] M. J. Frisch, G. W. Trucks, H. B. Schlegel, G. E. Scuseria, M. A. Robb, J. R. Cheeseman, G. Scalmani, V. Barone, B. Mennucci, G. A. Petersson, H. Nakatsuji, M. Caricato, X. Li, H. P. Hratchian, A. F. Izmaylov, J. Bloino, G. Zheng, J. L. Sonnenberg, M. Hada, M. Ehara, K. Toyota, R. Fukuda, J. Hasegawa, M. Ishida, T. Nakajima, Y. Honda, O. Kitao, H. Nakai, T. Vreven, J. A. Montgomery Jr., J. E. Peralta, F. Ogliaro, M. Bearpark, J. J. Heyd, E. Brothers, K. N. Kudin, V. N. Staroverov, T. Keith, R. Kobayashi, J. Normand, K. Raghavachari, A. Rendell, J. C. Burant, S. S. Iyengar, J. Tomasi, M. Cossi, N. Rega, J. M. Millam, M. Klene, J. E. Knox, J. B. Cross, V. Bakken, C. Adamo, J. Jaramillo, R. Gomperts, R. E. Stratmann, O. Yazyev, A. J. Austin, R. Cammi, C. Pomelli, J. W. Ochterski, R. L. Martin, K. Morokuma, V. G. Zakrzewski, G. A. Voth, P. Salvador, J. J. Dannenberg, S. Dapprich, A. D. Daniels, O. Farkas, J. B. Foresman, J. V. Ortiz, J. Cioslowski, and D. J. Fox, computer code GAUSSIAN 09, revision C.01, Gaussian Inc., Wallingford, CT, 2010.
- [31] C. Walther, G. Dietrich, W. Dostal, S. Krückeberg, K. Lützenkirchen, and L. Schweikhard, *Eur. Phys. J. D* **9**, 455 (1999).
- [32] Q.-M. Ma, Z. Xie, J. Wang, Y. Liu, and Y.-C. Li, *Phys. Lett. A* **358**, 289 (2006).
- [33] A. Sebetci, *Chem. Phys.* **354**, 196 (2008).
- [34] S. Peredkov, M. Neeb, W. Eberhardt, J. Meyer, M. Tombers, H. Kampschulte, and G. Niedner-Schatteburg, *Phys. Rev. Lett.* **107**, 233401 (2011).
- [35] M. Lange, M. W. Froese, S. Menk, D. Bing, F. Fellenberger, M. Grieser, F. Laux, D. A. Orlov, R. Repnow, T. Sieber, Y. Toker, R. v. Hahn, A. Wolf, and K. Blaum, *New J. Phys.* **14**, 065007 (2012).
- [36] H. T. Schmidt, R. D. Thomas, M. Gatchell, S. Rosén, P. Reinhard, P. Löfgren, L. Brännholm, M. Blom,

- M. Björkhage, E. Bäckström, J. D. Alexander, S. Leontein, D. Hanstorp, H. Zettergren, L. Liljeby, A. Källberg, A. Simonsson, F. Hellberg, S. Mannervik, M. Larsson, W. D. Geppert, K. G. Rensfelt, H. Danared, A. Paál, M. Masuda, P. Halldén, G. Andler, M. H. Stockett, T. Chen, G. Källersö, J. Weimer, K. Hansen, H. Hartman, and H. Cederquist, *Rev. Sci. Instrum.* **84**, 055115 (2013).
- [37] R. von Hahn, A. Becker, F. Berg, K. Blaum, C. Breitenfeldt, H. Fadil, F. Fellenberger, M. Froese, S. George, J. Göck, M. Grieser, F. Grussie, E. A. Guerin, O. Heber, P. Herwig, J. Karthein, C. Krantz, H. Kreckel, M. Lange, F. Laux, S. Lohmann, S. Menk, C. Meyer, P. M. Mishra, O. Novotný, A. P. O'Connor, D. A. Orlov, M. L. Rappaport, R. Repnow, S. Saurabh, S. Schippers, C. D. Schröter, D. Schwalm, L. Schweikhard, T. Sieber, A. Shornikov, K. Spruck, S. Sunil Kumar, J. Ullrich, X. Urbain, S. Vogel, P. Wilhelm, A. Wolf, and D. Zajfman, *Rev. Sci. Instrum.* **87**, 063115 (2016).

Long-term monitoring of the internal energy distribution of isolated cluster systems

Christian Breitenfeldt^{1,2}, Klaus Blaum², Sebastian George², Jürgen Göck²,
 Gregorio Guzmán-Ramírez³, Jonas Karthein², Thomas Kolling⁴, Michael Lange², Sebastian Menk²,
 Christian Meyer², Jennifer Mohrbach⁴, Gereon Niedner-Schatteburg⁴, Dirk Schwalm^{2,5,†},
 Lutz Schweikhard¹, and Andreas Wolf²

¹*Institut für Physik, Ernst-Moritz-Arndt-Universität, 17487 Greifswald, Germany;* ²*Max-Planck-Institut für Kernphysik, 69117 Heidelberg, Germany;* ³*Departamento de Ingenierías, Centro Universitario de Tonalá, Universidad de Guadalajara, Jal. 48525, Mexico;* ⁴*Fachbereich Chemie, Universität Kaiserslautern, 67663 Kaiserslautern, Germany;* ⁵*Department of Particle Physics, Weizmann Institute of Science, Rehovot 76100, Israel;* [†]*deceased 14 July 2016*

In this Supplemental Material, we first discuss the calculation of the delayed electron emission rate by vibrational autodetachment and the determination of its main parameters for Co_4^- from measurements. We also discuss the reliability of the determined parameters and present further details on the analysis procedure of the experimental internal energy distributions.

1 Delayed vibrational autodetachment model

1.1 Determination of the rate constant

Previous studies [1–4] have analyzed the delayed electron emission by vibrational autodetachment as the inverse process of electron capture on a polyatomic neutral target, using a statistical description. We apply this method to predict the decay rate constant k for anionic clusters of a given internal energy which arises either from the cluster production in the ion source or, additionally, from the one-photon excitation to $E' = E + h\nu$, where E is the anion cluster energy before excitation and $h\nu$ the photon energy.

The anionic cluster can detach its excess electron if its internal energy exceeds the adiabatic electron affinity (E_{EA}) of the neutral. The decay constant for delayed electron emission by vibrational autodetachment can be calculated by detailed balance [1, 5]:

$$k(E') = \frac{2m}{\pi^2 \hbar^3} \int \sigma_{\text{att}}(\epsilon) \epsilon \frac{\rho_n(E' - E_{\text{EA}} - \epsilon)}{\rho_a(E')} d\epsilon, \quad (\text{S1})$$

with ϵ being the kinetic energy of the detached electron, σ_{att} the cross section for attachment of an electron to the neutral cluster, and ρ_n and ρ_a the vibrational energy densities of states of the neutral and anionic system, respectively. While electron attachment by vibrationally inelastic collisions has been calculated for better known polyatomic systems such as SF_6 [6], detailed predictions for the electron attachment cross section of Co_4 are not available. Instead, we approximate the capture cross section σ_{att} by the Langevin expression [1]

$$\sigma_L = \pi \sqrt{\frac{2\alpha e^2}{\epsilon}}, \quad (\text{S2})$$

(with α being the polarizability of the neutral cluster) multiplied by an energy-independent sticking coefficient p_s :

$$\sigma_{\text{att}} = p_s \sigma_L. \quad (\text{S3})$$

The sticking probability p_s takes into account that for electron attachment, energy has to be transferred from the electron to the vibrational modes of the cluster. Thus, p_s can be as low

as 0.001 [1]. As p_s is unknown we express the decay constant, up to an energy-independent factor, by

$$w(E') = \int_0^{E'-E_{\text{EA}}} \sqrt{\epsilon} \frac{\rho_n(E' - E_{\text{EA}} - \epsilon)}{\rho_a(E')} d\epsilon. \quad (\text{S4})$$

The overall size of the decay rate constant we specify by its value k_0 at an anionic cluster internal energy of $E'_0 = E_{\text{EA}} + 1 \text{ meV}$. We make this choice of E'_0 as 1 meV is the energy resolution of the calculations and, thus, $E'_0 = E_{\text{EA}} + 1 \text{ meV}$ the lowest energy for which k is non-zero. The decay constant is then described by

$$k(E') = k_0 \frac{w(E')}{w(E'_0)} \quad (\text{S5})$$

where a constant factor from Eqs. (S2) and (S3) has been taken out of the integral of Eq. (S1). k_0 then is a scaling factor with a fixed functional shape expressed by Eq. (S4). The experimental determination of k_0 and E_{EA} is described in Secs. 1.2 and 1.3.

The calculation assumes that on the time scale investigated (decay rates of $< 10^6 \text{ s}^{-1}$) the only effective process for autodetachment is the coupling of electronic and vibrational motion (correspondingly, the cluster's internal energy in electron attachment is via vibrational excitation only). This leads to the concept of vibrational autodetachment [1]. Electronic and rotational excitation of the Co_4 system are assumed not to change in this process. Consequently, these other excitations cancel in the ratio of the densities of states for the reaction rate. It is the large number of vibrational levels in the neutral cluster that acts as a reservoir for the low-rate, statistical process. Direct detachment by electronic excitation will give rise to a prompt neutralization signal that is not considered in this experiment. Fine-structure excitation may contribute to the energy available for a statistical excitation of the Co_4^- vibrations, but is considered here not to directly drive electron detachment processes. Hence, we use the vibrational energy level densities in Eq. (S1).

The required vibrational densities of states were derived with the harmonic-oscillator approach using the algorithm by Beyer and Swinehart [7]. The vibrational frequencies required for this step were calculated by density-functional theory (DFT) and are listed in Table S1.

Once the energy dependent autodetachment rate can be predicted with Eq. (S5), the neutral event rate can be calculated as a function of time t as

$$R(t) = C_1 \int_0^\infty N(E') k(E') e^{-[k(E') + k_r]t} dE' + C_2, \quad (\text{S6})$$

where $N(E')$ is the distribution of vibrational energies in the anion and $C_{1,2}$ are constants adjusting the total scale of the decay as well as the collisional background. The additional

Table S1: Wave numbers (in cm^{-1}) of the six vibrational modes (n) of neutral Co_4 (ν_n^{neut}) and the anionic Co_4^- (ν_n^{ani}). DFT calculations were realized with the GAUSSIAN program [8]. From various geometries and spin multiplicities tested, the geometries of the lowest binding energy (including the zero-point energy) and the lowest spin multiplicity were chosen (nonet for the neutral and decuplet for the anion). The wave numbers of other geometries are similar in size (generally within $\sim 20\%$, up to $\sim 60\%$ for ν_2).

n	1	2	3	4	5	6
ν_n^{neut}	78	171	187	203	283	322
ν_n^{ani}	85	138	210	217	296	304

rate k_r takes into account radiative decays of excited levels with a vibrational energy of $E' \approx E_{\text{EA}}$. Typical values of k_r lie between 10 and 100 s^{-1} [4]. For the case of initial internal energy of cluster anions in the ion source, $E' = E$ (distributed over the vibrational degrees of freedom) and t is the time after the ion production in the source. For the case of an already relaxed anionic cluster and subsequent one-photon excitation by a laser pulse, followed by redistribution of the excitation energy over the vibrational degrees of freedom, $E' = E + h\nu$, where E is the internal anionic cluster energy before the excitation and $h\nu$ the photon energy, while t is replaced by the delay time $\tau = t - t_p$ from the laser pulse at time t_p .

1.2 Analysis of the vibrational autodetachment rate: initial thermal energy

The initial thermal energy in the ion source results in vibrational excitation modeled by the canonic energy distribution

$$N(E) = C_0 \rho_a(E) e^{-E/k_B T}, \quad (\text{S7})$$

where C_0 is a normalization factor and $\rho_a(E)$ the anionic vibrational density of states. We set $T = T_i$ with T_i being the initial (i.e., the ion source) temperature. The time dependence of electron emission and, thus, the neutral event rate is then calculated by Eq. (S6) with $E' = E$.

Similar to previous work on SF_6^- molecules [4], we measured the time dependence of the neutral event rate for Co_4^- with high precision (see the upper panel of Fig.S1) under

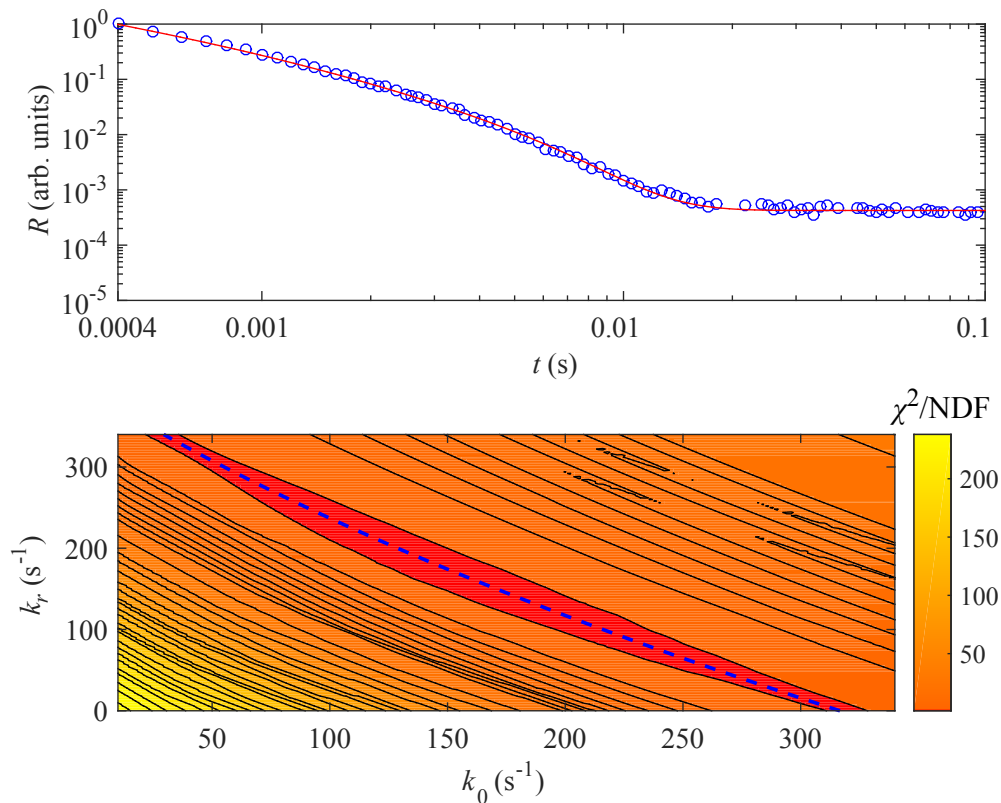


Figure S1: Top panel: Initial decay curve of Co_4^- (open circles) and fitted line (red) with $T=1500$ K, $k_r = 70 \text{ s}^{-1}$, $E_{\text{EA}}=1.73$ eV and $k_0 = 240 \text{ s}^{-1}$. Bottom panel: χ^2/NDF of the fit of the initial decay after production with the MISS for $E_{\text{EA}}=1.73$ eV and $T_i =1500$ K. The dashed blue line is the quadratic fit to the correlation between k_r and k_0 . (See the text for further discussion.)

almost background free conditions achieved by operating the EIBT at 15 K (for this particular measurement). This makes it possible to follow the vibrational autodetachment down to very small rates, corresponding to excitation energies just above E_{EA} [see the upper panel of Fig. S1]. We take care to define t as the sum of the storage time and the time of flight from the ion source to the trap ($\sim 90 \mu\text{s}$).

In fitting Eq. (S6), the parameters $C_{1,2}$, k_0 and k_r as well as T_i and E_{EA} were varied. The quality of the fit was almost independent of T_i and E_{EA} , tested over ranges of 1300–2500 K and 1.65–1.78 eV, respectively. Regarding k_0 and k_r , the quality of fit, as represented by the reduced variance χ^2/NDF , is shown in Fig. S1 (bottom panel) (here, $T_i = 1500$ K and $E_{\text{EA}} = 1.73$ eV). Minimum χ^2/NDF is obtained for combinations of k_0 and k_r which can be quantified by a quadratic expression (dashed blue line). The individual values of k_0 and k_r cannot be extracted from these data alone. However, their sum is approximately constant and quite precisely constrained [e.g., $k_0 + k_r = 310(10) \text{ s}^{-1}$ in the expected range of $k_r \lesssim 100 \text{ s}^{-1}$]. The fact that with the cryogenic EIBT the dependence of the vibrational autoionization rate can be followed over many orders of magnitude yields the high precision of $k_0 + k_r$. Because of the broad-band excitation it can be understood that, in contrast to the laser excitation discussed below, the fit results show little sensitivity on E_{EA} .

1.3 Analysis of the electron affinity: laser excitation

The time and photon-energy dependence of the laser-induced delayed signals in Fig. 2 of the main paper allow to delimit the value of E_{EA} . The time dependence of the neutral rate follows Eq. (S6) with $E' = E + h\nu$. At long storage times (t), when the yields Y in delay window 1 become similar for both ion sources [main paper, Fig. 2(a) and (b)], the laser-induced signal as a function of $h\nu$ first appears when going down from $h\nu = 1.88$ eV to 1.77 eV. We conclude that, after one-photon absorption at 1.88 eV, E' is too high (and the decay too fast, even for the smallest initial energy E) to yield a signal in delay window 1. However, for $h\nu = 1.77$ eV some anions with initial energies $E \sim 0$ overlap after laser excitation with the energy band which is sensitive to delayed autodetachment [main paper, Fig. 2(d)]. The decay signal is expected, on the one hand, to depend on the position of the lower edge of the shifted energy distribution (near 1.77 eV) with respect to E_{EA} . On the other hand, only the lowest part of the shifted energy distribution lies in the sensitive range (corresponding to the observed decay times of $\geq 12 \mu\text{s}$) and, hence, the decay behaviour at these times will depend only little on the thermal energy of the anions before excitation. We hence analyze the time dependence for $h\nu = 1.77$ eV and use the data with the highest yield at this $h\nu$, taken for the cold (LVAP) ion source (see Fig. 2 of the main paper). To ensure sufficient statistics and to minimize storage-time dependent fluctuations, we average the laser-induced decay time dependences over all LVAP data for the nearly stable conditions at later storage times (>3.8 s).

To the data (see Fig. S2, upper panel) we fit the time dependence of Eq. (S6) by adjusting C_1 and C_2 while varying E_{EA} from 1.66 eV to 1.77 eV and k_0 from 30 s^{-1} to 315 s^{-1} (see bottom panel of Fig. S2). The range of small χ^2/NDF is rather well defined regarding E_{EA} . Especially, using the result from the cryogenic measurement of $k_0 + k_r = 310(10) \text{ s}^{-1}$ and considering the expected range of $k_r \lesssim 100 \text{ s}^{-1}$ (i.e., $k_0 \gtrsim 210 \text{ s}^{-1}$), we find $E_{\text{EA}} = 1.73(1) \text{ eV}$. Note that this calibration yields the result that E_{EA} lies below the well known photon energy of $h\nu = 1.77$ eV by 0.04(1) eV. A shallow minimum of χ^2/NDF as a function of the parameter k_0 shows that $k_0 = 240(70) \text{ s}^{-1}$, which implies $k_r = 70(70) \text{ s}^{-1}$. The uncertainty in k_0 has little influence on the derived internal energy distribution (estimated below), since the latter is measured through a scan of the laser frequencies.

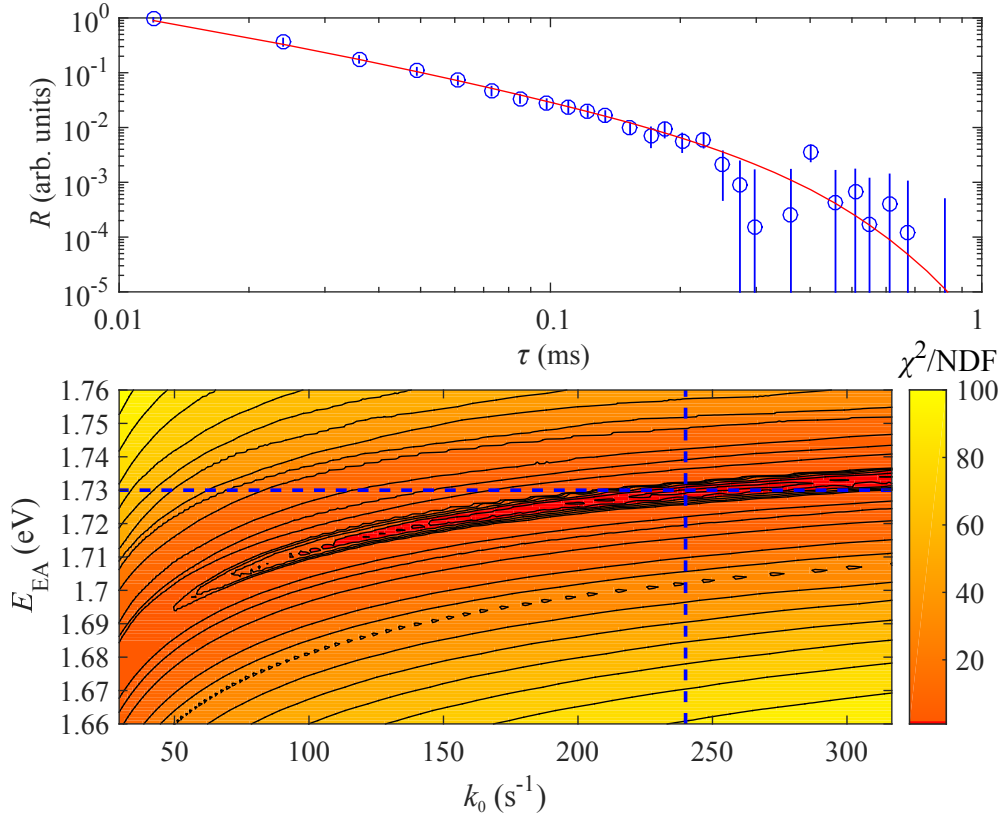


Figure S2: Top panel: Measured decay curve after excitation with photons with $h\nu = 1.77$ eV (open circles). The ions were produced with the LVAP. All data between 3.8 and 4.7 s storage time are summed up. The curve shows a fit with the parameters given below. Bottom panel: χ^2/NDF of the fitted laser induced delayed electron detachment curve for various combinations of the parameters E_{EA} and k_r . The dashed horizontal and vertical lines mark $k_0 = 240 \text{ s}^{-1}$ and $E_{\text{EA}} = 1.73 \text{ eV}$.

The DFT calculations resulted in a polarizability of $\alpha = 29 \text{ \AA}$. Using this value to calculate the sticking probability results in $p_s = 3(1)\%$, which is a reasonable value [1].

2 Experimental internal energy distributions

2.1 Detection probability function and energy bins

For cluster anions excited to energy E' we give the probability of leading to a neutralization event at the detector in the time interval $I_\tau = [\tau_1, \tau_2]$ after a laser pulse as

$$\begin{aligned}
 p(E', I_\tau) &= \frac{1}{2} \int_{\tau_1}^{\tau_2} k(E') e^{-[k(E') + k_r]\tau} d\tau \\
 &= \frac{k(E')}{2[k(E') + k_r]} \left(e^{-[k(E') + k_r]\tau_1} - e^{-[k(E') + k_r]\tau_2} \right). \quad (\text{S8})
 \end{aligned}$$

As functions of E' these probability functions are shown in Fig. S3 [see also Fig. 1(d) of the main paper]. The energy bin assigned if an event is detected within a given time window is defined as follows. First, limits are found that contain 95% of the area for each the $p(E')$ curves that belong to delay window 1 or 2, respectively. Window 1 leads to the upper energy

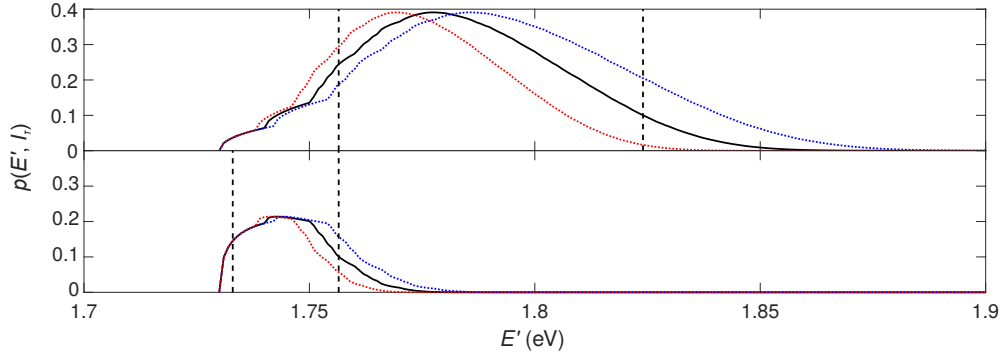


Figure S3: Probability functions $p(E', I_\tau)$ for $I_{\tau,1} = [12 \mu s, 200 \mu s]$ (upper panel) and $I_{\tau,2} = [400 \mu s, 1500 \mu s]$ (lower panel). The black curves are identical to Fig. 1(d) of the main paper. The bin limits (dashed vertical lines) belong to these curves. For the red (blue) curves the vibrational frequencies were reduced (increased) by 20%.

(E') interval and window 2 to the lower one (Fig. S3). The upper limit of the upper E' interval and lower limit of the lower E' interval (“outer limits”) are retained. At the inner limits, the energy intervals overlap; hence, the upper limit of the lower interval is shifted down and the lower limit of the upper interval shifted up until they are only 1 meV apart and exclude equal relative amounts of the $p(E')$ areas. This leads to the limits listed in Table S2. The relative amounts of area excluded by the inner limits are 13% for each of the two intervals.

In this derivation, the energies are essentially defined relative to E_{EA} as given by the last column of Table S2. The shifts of the limits occurring when the vibrational frequencies of the model are reduced or increased by 20% are illustrated by Fig. S3. Approximately, the bin limits of $I_{E'-E_{EA}}$ shift by about $\pm 20\%$.

The intervals of internal anionic cluster energies E are obtained from the limits of $I_{E'-E_{EA}}$ by subtracting the quantity $h\nu - E_{EA}$. Hence, the energy accuracy for the bins of the internal energy distribution is given by the accuracy in E_{EA} , amounting to ± 0.01 eV. Through a $\pm 20\%$ inaccuracy in the vibrational frequencies the average position of the bin related to window 1 may in addition shift by about ± 0.01 eV. From this, we state an estimated overall uncertainty of about ± 0.02 eV for the internal energy bins. (Clearly, values $E < 0$, which may occur for $h\nu = 1.77$ eV, are eliminated from the analysis by letting the corresponding bin start at $E = 0$.)

We have also investigated the sensitivity of the complete analysis procedure leading to the final average internal energy \bar{E}_{eq} [Eq. (1) of the main paper] on the precise choice of the parameter k_0 . By varying $k_0 = 240(70) \text{ s}^{-1}$ within its uncertainty range (between 160 s^{-1} and 300 s^{-1}), we find a variation of \bar{E}_{eq} between 0.167 eV and 0.158 eV, respectively. ($\bar{E}_{eq} = 0.162$ eV for $k_0 = 240 \text{ s}^{-1}$.) From this, estimate that the uncertainty at which k_0 can be

Table S2: Windows in the delay time, I_τ , the energy after excitation, $I_{E'}$ for $E_{EA} = 1.73$ eV, and the energy windows relative to E_{EA} , $I_{E'-E_{EA}}$. The limits of I_τ are given in μs and those of $I_{E'}$ and $I_{E'-E_{EA}}$ in eV. The parameter uncertainties yield (see Fig. S3) a $\pm 20\%$ uncertainty for the limits of $I_{E'-E_{EA}}$ (third column).

Window no.	I_τ	$I_{E'}$	$I_{E'-E_{EA}}$
1	[12, 200]	[1.757, 1.824]	[0.024, 0.094]
2	[400, 1500]	[1.733, 1.756]	[0.003, 0.023]

experimentally determined leads to a $\pm 3\%$ uncertainty of the internal energy scale (± 0.005 eV on \bar{E}_{eq}).

Taken together both influences discussed in this Section, we state the systematical uncertainty of the internal energy through the model for the sensitive E' windows as ± 0.02 eV. As described below, possible unaccounted variations of the photon absorption cross section lead to additional independent systematic uncertainty of about the same size. From this, we quote the systematic uncertainty of the final average internal energy \bar{E}_{eq} as ± 0.03 eV. All uncertainties given are to be understood as single standard deviations.

2.2 Shape of the energy distribution function and photon absorption cross section

Experimental parameters such as the detection efficiency do not affect the distribution function as they can be assumed to be independent of the photon energy and constant during the measurement; their absolute amount is eliminated by normalizing the binned internal energy distributions in a final step. Moreover, normalization to variations in the stored ion is assured within an estimated uncertainty of 20%.

The largest uncertainty in the shape of the internal energy distributions is due to the photon absorption cross section $\sigma(\nu)$ of Co_4^- , which is assumed to be independent on the photon energy in the range of ~ 1.8 eV to ~ 1.1 eV. The functional dependence $\sigma(\nu)$ influences both the derived energy distributions (Fig. 3 of the main paper) and the derived mean energy (main paper, Fig. 5).

No experimental absorption cross sections $\sigma(\nu)$ are available for this system. For comparable metal clusters, an energy dependence was observed. Thus, in case of V_{13}^+ the cross section increases with photon energy [9], the data being well reproduced by Mie theory. Applying Mie theory to Co_4^- , the cross section is predicted to monotonously increase by a factor of four over the photon energy range investigated. In contrast, for Al_4^- a cross section decreasing with photon energy was observed [2]. Sharp resonances are unlikely to occur considering the vibrational configuration space and the high density of vibrationally excited levels.

As the energy bins in E are the constant intervals $I_{E'}$ from Table S2, shifted down by $h\nu$, any given energy E corresponds to a certain value of $h\nu$. Therefore, variations of $\sigma(\nu)$ should produce the same E -dependent modification factor for each of the distributions in Fig. 3 of the main paper. As no clear repeating structures are observed in the various distributions and lacking better options, we choose to assume a constant photon excitation rate. However, smooth factor-of-four variations of $\sigma(\nu)$ could occur as mentioned above.

To model possible effects of a smooth variation of $\sigma(\nu)$, we calculated its possible effect on a canonical energy distribution near the measured equilibrium internal energy \bar{E}_{eq} . We calculate these distributions from Eq. (S7) with the vibrational level density $\rho_a(E)$ from the harmonic parameters of Table S1 and apply the experimental binning. Calculating the average of E with this binned distribution we find, at $T = 295$ K, $\bar{E} = 0.0942$ eV. The unbinned average (i.e. with the 1 cm^{-1} binning of the calculated $\rho_a(E)$, negligibly small compared to the experimental bins) we find as $\bar{E} = 0.0896$ eV. Hence, the experimental binning alone shifts the measured average energy up compared to the unbinned case by 0.0046 eV.

We then define a correction factor of 1 at $h\nu = E_{\text{EA}} = 1.73$ eV ($E = 0$) and of either $1/4$ or 4 at $h\nu = 0.90$ eV ($E = 0.83$ eV), varying linearly with E between these limits, to simulate the possible variations of $\sigma(\nu)$ according to the previous discussion. We multiply the bin contents with the correction factors for both cases, taken at the bin centers, and calculate the average E of the corrected distributions. At $T = 295$ K, \bar{E} changes by -0.0036 eV for a

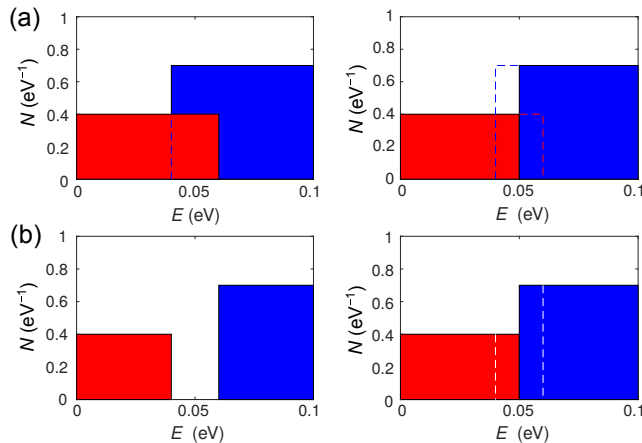


Figure S4: Redefinition of the energy bins to avoid overlaps (a) and gaps (b) in the energy distribution. The left and right diagrams show the bin boundaries before and after the adjustment, respectively. See text for details.

reduction and $+0.0134$ eV for an increase of the correction factor along E [hence, a change of $\sigma(\nu)$ as ν decreases]. In the region of $\bar{E}_{\text{eq}} = 0.162$ eV (canonical $T = 436$ K) the binning effect is $+0.0043$ eV and the shifts by factor-of-four sensitivity variations are -0.0083 eV and $+0.0180$ eV for a reduction and increase along E , respectively. We approximate our uncertainty estimate through a factor-of-four variation of $\sigma(\nu)$ by a symmetric range of ± 0.02 eV.

2.3 Binning the energy distribution

The photon energies used were non-equidistant. Thus, considering the bins of the internal energy distribution function, some ranges of E are not probed at all, while others are probed by two different wavelengths. For reconstructing the energy distribution continuously and uniquely, the following adjustments were made: When the upper edge of the previous bin in E lies above the lower edge of the next one, as in Fig. S4(a), a new boundary where the two bins are touching each other is placed half way within the overlap region, reducing the width of each bin by the same amount. Conversely, when the upper edge of the previous bin lies below the lower edge of the next one, Fig. S4(b), a new boundary where the two bins are touching each other is placed half way within the gap, increasing the width of each bin by the same amount. In both cases, the value of the distribution function within the bin is left unchanged. In a final step the energy distributions were normalized by applying a factor to the energy distribution such that

$$\sum_{\tilde{I}_E} N(\tilde{I}_E) \Delta E(\tilde{I}_E) = 1 \quad (\text{S9})$$

with the adjusted bins \tilde{I}_E .

References

- [1] J. U. Andersen, E. Bonderup, and K. Hansen, *J. Phys. B: At. Mol. Opt. Phys.* **35**, R1 (2002).
- [2] B. Kafle, O. Aviv, V. Chandrasekaran, O. Heber, M. L. Rappaport, H. Rubinstein, D. Schwalm, D. Strasser, and D. Zajfman, *Phys. Rev. A* **92**, 052503 (2015).

- [3] S. Martin, J. Bernard, R. Brédy, B. Concina, C. Joblin, M. Ji, C. Ortega, and L. Chen, *Phys. Rev. Lett.* **110**, 063003 (2013).
- [4] S. Menk, S. Das, K. Blaum, M. W. Froese, M. Lange, M. Mukherjee, R. Repnow, D. Schwalm, R. von Hahn, and A. Wolf, *Phys. Rev. A* **89**, 022502 (2014).
- [5] K. Hansen, *Statistical Physics of Nanoparticles in the Gas Phase*, Springer Series on Atomic, Optical and Plasma Physics No. 73 (Springer, 2013).
- [6] J. Troe, T. M. Miller, and A. A. Viggiano, *J. Chem. Phys.* **127**, 244303 (2007).
- [7] T. Beyer and D. F. Swinehart, *Commun. ACM* **16**, 379 (1973).
- [8] M. J. Frisch, G. W. Trucks, H. B. Schlegel, G. E. Scuseria, M. A. Robb, J. R. Cheeseman, G. Scalmani, V. Barone, B. Mennucci, G. A. Petersson, H. Nakatsuji, M. Caricato, X. Li, H. P. Hratchian, A. F. Izmaylov, J. Bloino, G. Zheng, J. L. Sonnenberg, M. Hada, M. Ehara, K. Toyota, R. Fukuda, J. Hasegawa, M. Ishida, T. Nakajima, Y. Honda, O. Kitao, H. Nakai, T. Vreven, J. A. Montgomery Jr., J. E. Peralta, F. Ogliaro, M. Bearpark, J. J. Heyd, E. Brothers, K. N. Kudin, V. N. Staroverov, T. Keith, R. Kobayashi, J. Normand, K. Raghavachari, A. Rendell, J. C. Burant, S. S. Iyengar, J. Tomasi, M. Cossi, N. Rega, J. M. Millam, M. Klene, J. E. Knox, J. B. Cross, V. Bakken, C. Adamo, J. Jaramillo, R. Gomperts, R. E. Stratmann, O. Yazyev, A. J. Austin, R. Cammi, C. Pomelli, J. W. Ochterski, R. L. Martin, K. Morokuma, V. G. Zakrzewski, G. A. Voth, P. Salvador, J. J. Dannenberg, S. Dapprich, A. D. Daniels, O. Farkas, J. B. Foresman, J. V. Ortiz, J. Cioslowski, and D. J. Fox, computer code GAUSSIAN 09, revision C.01, Gaussian Inc., Wallingford, CT, 2010.
- [9] C. Walther, G. Dietrich, W. Dostal, S. Krückeberg, K. Lützenkirchen, and L. Schweikhard, *Eur. Phys. J. D* **9**, 455 (1999).